J. Biochem. **139**, 989–996 (2006)
doi:10.1093/jb/mvj111

Aggregation of Partially Unfolded Myosin Subfragment-1 into Spherical Oligomers with Amyloid-Like Dye-Binding Properties

Hideyuki Komatsu[1,2,*], Nami Shinotani[1], Yoshitaka Kimori[1], Jun-ichiro Tokuoka[1], Kuniyoshi Kaseda[1], Hiroyuki Nakagawa[1] and Takao Kodama[1]

[1]*Department of Bioscience and Bioinformatics, Kyushu Institute of Technology, Iizuka, Fukuoka, 820-8502; and* [2]*Institute for Materials Chemistry and Engineering, Kyushu University, Fukuoka, Fukuoka, 812-8581*

Received February 21, 2006; accepted April 3, 2006

Proteolytic myosin subfragment 1 (S1) is known to be partially unfolded in its 50-kDa subdomain by mild heat treatment at 35°C [Burke *et al.* (1987) *Biochemistry* 26, 1492–1496]. Here, we report that this partial unfolding is accompanied by aggregation of S1 protein. Characteristics of the aggregate thus formed were: (i) formation of transparent sediment under centrifugation at 183,000 × *g*; (ii) amyloid-like, dye-binding properties such as Congo red–binding and Thioflavin T fluorescence enhancement; (iii) a uniformly sized spherical appearance in electron micrographs; and (iv) sensitivity to tryptic digestion. Gel filtration analysis of the aggregation process indicates that the spheroid was formed through an intermediate oligomeric stage. The aggregate inhibited spontaneous aggregation of an isolated 50 kDa fragment into a large amorphous mass. The remaining native regions in the partially unfolded S1 were probably responsible for this effect. These results show that, unlike the 50-kDa fragment, the partially unfolded S1 molecules do not form amorphous aggregates but assemble into spherical particles. The native regions in partially unfolded S1 may be a determinant of aggregate morphology.

Key words: amyloid, myosin subfragment-1, partial unfolding, protein aggregation.

Abbreviations: CD, circular dichroism; DTT, dithiothreitol; HPLC, high performance liquid chromatography; MOPS, 3-morpholinopropanesulfonic acid; PIPES, piperazine-1,4-bis (2-ethanesulfonic acid); S1, myosin subfragment 1; SDS-PAGE, sodium dodecyl sulfate–polyacrylamide gel electrophoresis; ThioT, Thioflavin T.

Protein fibrillar aggregates are recognized as a pathological hallmark of amyloid diseases, such as Alzheimer's disease, Parkinsonism, familial amyloid polyneuropathy and senile systemic amyloidosis (*1*). Recently, however, amyloid-like fibrillization of non-disease-related proteins has also been reported, suggesting that such fibril formation is a rather general property of proteins (*2–6*). Amyloid formation is known to be a three-step process (*7*, *8*). Protein molecules first undergo partial unfolding, accompanied by an increase in β-sheet content (partial unfolding), then associate with each other to form oligomers, called nuclei or pre-fibrillar aggregates (intermediate-formation), and finally assemble into fibrils (fibrillization).

As regards the etiology of amyloid diseases, a more prominent role of nonfibrillar oligomerization over fibrillization of amyloid protein has recently been pointed out, which shows that nonfibrillar oligomers, but not fibrils, are neurotoxic (*9–16*). In contrast with extensive studies of fibrillization, however, little is known about nonfibril-type aggregations, which are often encountered in protein experiments, but usually regarded as a nuisance or of no academic value. Aggregations of genetically expressed and chemically synthesized proteins are a major obstruction to protein engineering (*17–20*). Thus, a successful strategy for prevention of aggregation will have useful applications (*21*). Toward this end, characterization of various types of aggregations acquires significance. In this paper, we describe the oligomer formation of myosin subfragment-1 (S1) as a novel type of protein aggregation model *in vitro*.

S1 is a proteolytic fragment (115 kDa) of the myosin molecule, which corresponds to its globular portion, consisting of a heavy chain (95 kDa) and one light chain (20 kDa) (*22*). The heavy chain is composed of N-terminal (25 kDa), middle (50 kDa) and C-terminal (20 kDa) subdomains (*23*). These three subdomains constitute the ATP- and actin-binding sites which hydrolyze ATP and interact cooperatively with actin. While studying the function of the 50-kDa subdomain, some research groups have found that mild heat treatment, incubation of S1 at 35°C, induces partial unfolding in this subdomain (*24–26*). This partially unfolded S1 can bind ATP and actin but not hydrolyze ATP. We here report that this partially unfolded S1 aggregates into a protease-sensitive, spherical oligomer having some amyloid-like properties. Kinetics of the aggregation and interaction with the isolated 50-kDa fragment are also described.

MATERIALS AND METHODS

Preparation of Proteins—Rabbit skeletal myosin was prepared as described elsewhere (*27*) and digested with chymotrypsin to prepare S1 (*28*). The concentration of S1 was measured with an extinction coefficient of $E^{1\%} = 7.5\ cm^{-1}$ at 280 nm. The 50-kDa fragment of S1 was prepared according to the method of Muhlrad and Morales (*29*) and stored until use in 5 M guanidine-HCl,

*To whom correspondence should be addressed. Tel: +81-948-29-7845, Fax: +81-948-29-7801, E-mail: hide@bio.kyutech.ac.jp

5 mM EDTA, 5 mM DTT and 50 mM Tris-HCl, pH7.5. Its concentration was determined by the Bradford method (*30*).

Mild Heat Treatment of Myosin S1—S1 was dialyzed against 0.1 M KCl, 20 mM PIPES (pH 7.0) or 0.1 M KCl, 20 mM MOPS (pH 7.0) at 4°C and stored on ice until incubation at 35°C. Incubation was started by addition of S1 solution into 10–30 volumes of the buffer pre-incubated at 35°C. The protein concentration of S1 was 0.06–0.5 mg/ml. If necessary, samples were taken at intervals and stored on ice.

Evaluation of Partial Unfolding of S1—Samples were incubated at 35°C, as described above, and the degree of unfolding was evaluated by three methods. Firstly, limited proteolysis of incubated S1 (0.5 mg/ml) was performed using trypsin (w/w: 1:100) at 25°C for 30 min. After addition of soybean trypsin inhibitor, the digests were analyzed by SDS-PAGE. Secondly, the ATPase activity of incubated S1 (0.55 mg/ml) was measured at 25°C by the Taussky method (*31*). The reaction mixture consisted of 0.5 mg/ml S1, 0.4 mM ATP, 10 mM $MgCl_2$, 0.1 M KCl, and 20 mM MOPS (pH 7.0). Thirdly, circular dichroism (CD) of 0.26 mg/ml S1 incubated at 35°C in 10 mM potassium phosphate (pH 7.0) for 90 min was measured using a JASCO J-720 spectropolarimeter. The CD spectra were recorded using a 1-mm path length quartz cell at a spectrum range of 200–250 nm.

Monitoring of the Aggregation Process—Aggregation of S1 was monitored by the following three methods. Firstly, S1 stored on ice was added to 0.1 M KCl and 20 mM PIPES (pH 7.0) pre-incubated at 35°C, and the light scattering at 90° was monitored in the thermostatted cell at a wavelength of 600 nm. The protein concentration was 0.06–0.48 mg/ml. Secondly, incubated S1 (0.28 mg/ml) was withdrawn from the mixture at intervals for sedimentation assay. After centrifugation at 183,000 × *g* for 90 min at 4°C, protein concentration of the supernatant was measured by the Bradford method (*30*). Thirdly, samples stored on ice were added to 0.1 M KCl and 20 mM PIPES (pH 7.0) pre-incubated at 35°C, and the turbidity of 0.36 mg/ml S1 was monitored in thermostatted cells (35°C) at a wavelength of 350 nm.

Dye Staining of the Aggregate—Protein (0.4 mg/ml) was incubated at 35°C for 90 min, and then mixed with 5 μM Congo red. The absorbance spectra of samples were recorded at 350–650 nm. For observation by polarization light microscopy, S1 was incubated at 35°C for 90 min, and aggregates were sedimented at 183,000 × *g*. The precipitate was incubated with 50 μM Congo red at 25°C for 5 min, then washed three times with buffer (0.1 M KCl, 20 mM PIPES, pH 7.0). After washing with deionized water, the suspension was placed on a glass slide and dried at room temperature prior to microscopic observation. For Thioflavin T (ThioT) staining, S1 (0.1 mg/ml) was incubated at 35°C for 90 min and mixed with 5 μM ThioT. Fluorescence spectra were recorded at 25°C at 450–600 nm at an excitation wavelength of 440 nm.

Electron Microscopy and Its Image Analysis—S1 (0.5 mg/ml) was incubated at 35°C for 1.5, 7 and 12 h. Samples were absorbed onto carbon-coated copper grids, washed with deionized water, and negatively stained with uranyl acetate. Electron micrographs were taken using a JEOL 100CX-II transmission electron microscope at an accelerating voltage of 80 kV. The micrographs were digitized using an imaging scanner (EPSON GT9700-F; Tokyo, Japan). The digitized image was converted to a binary image to cancel out background noise. A discrete area was defined as a particle, the size of which was calculated from the number of pixels detected in the area.

Gel Filtration Analysis—S1 (0.48 mg/ml) was incubated at 35°C in 0.1 M KCl and 20 mM PIPES (pH 7.0). Samples were filtered through a 0.22-μm pore size membrane and applied to a TSK G3000SWXL column (TOSOH) attached to an HPLC system. The column was equilibrated with 0.1 M KCl and 20 mM PIPES (pH 7.0). The flow rate was 1 ml/min. The eluted protein was detected by absorbance at 280 nm. The molecular weight of each peak was estimated from the calibration curve, which was obtained from an elution pattern of a set of standard proteins (Sigma). The elution profiles were analyzed by the peak deconvolution method using the ORIGIN Curve Fitting Module. To fractionate each peak, S1 was incubated at 35°C for 40–50 min and subjected to gel filtration, by which the samples were separated into distinguishable peaks. Each peak was subjected to tryptic digestion followed by SDS-PAGE and spectrum analysis with Congo red, as described above.

Test of Trypsin Effect on Aggregation—After incubation of S1 (0.36 mg/ml) at 35°C for 3 h, the change in 90° light scattering associated with addition of trypsin (w/w, 1:100) was monitored at 25°C. In addition, S1 incubated at 35°C for 50 min was digested with trypsin (w/w, 1:100) at 25°C for 30 min, and the molecular mass of the digest was analyzed by gel filtration, as described above.

Monitoring of 50-kDa Fragment Aggregation—Time course of 50-kDa fragment aggregation was monitored at 25°C by measuring turbidity at 350 nm in 0.1 M KCl and 20 mM PIPES, pH 7.0. To start the aggregation, a solution of the 50-kDa fragment (2.7 mg/ml) in 5 M guanidine-HCl, 5 mM EDTA, 5 mM DTT and 50 mM Tris-HCl, pH 7.5, was diluted with 60 volumes of 0.1 M KCl and 20 mM PIPES, pH 7.0. The diluted solution was supplemented with 0.02 mg/ml (20% of the 50-kDa fragment in molar ratio) native or partially denatured S1, or 0.0088 mg/ml (20% of the 50-kDa fragment in molar ratio) seed of the 50-kDa fragment aggregate. For preparation of the seed, the 50-kDa fragment (0.044 mg/ml) was incubated at 25°C for 3 h, stored at 4°C overnight, then sonicated.

RESULTS

Partial Unfolding of S1—We confirmed the specific unfolding of the 50-kDa subdomain by mild heat treatment, as previously reported by others (*26–28*). The SDS-PAGE pattern of limited tryptic digestion of native S1 (Fig. 1A, incubation time, 0 min) revealed three major fragments (50, 25 and 20 kDa) corresponding to the subdomains of S1. The intensity of the 50-kDa band decreased as the incubation time at 35°C increased, whereas the intensity of 25- and 20-kDa bands was not significantly affected by incubation time. Concomitantly with this unfolding, myosin S1 ATPase activity decreased with first-order kinetics, although it did not decrease at a temperature of 25°C (Fig. 1B). All three subdomains unfolded together when incubated at >40°C (data not shown). Thus, the 50-kDa unfolding

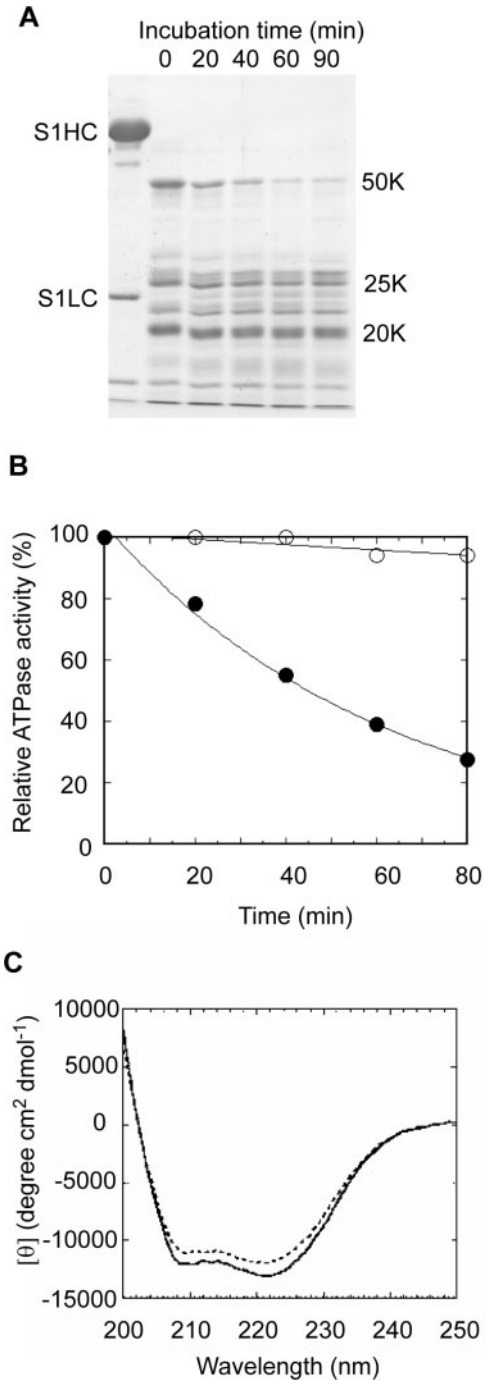

Fig. 1. **Partial unfolding of S1.** (A) Limited tryptic proteolysis analysis. Incubated S1 was subjected to limited tryptic digestion and applied to SDS-PAGE. S1HC, S1LC, 50K, 25K and 20K indicate heavy and light chains of S1 and 50-, 25- and 20-kDa subdomains, respectively. Incubation time is shown above the gel. (B) ATPase inactivation. Open and closed circles indicate activity of S1 incubated at 25 and 35°C, respectively. (C) Change of CD spectrum of S1. Solid and dashed lines indicate native and mild heat–treated (35°C for 90 min) S1, respectively.

with concomitant ATPase loss occurs at a temperature of ~35°C.

The CD signals of mild heat–treated S1 showed a small increase in wavelength from 205 to 235 nm (Fig. 1C),

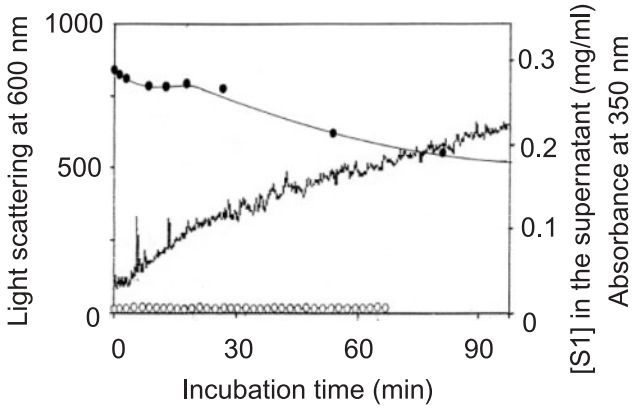

Fig. 2. **Time course of S1 aggregation at 35°C.** Solid line shows light scattering at 600 nm. Open and closed circles indicate turbidity at 350 nm and S1 concentration of supernatant after centrifugation, respectively. The concentration of S1 was 0.28 mg/ml for light scattering and sedimentation assay and 0.36 mg/ml for turbidity measurement.

indicating a slight decrease of α-helical content in the 50-kDa subdomain accompanying the partial unfolding. The CD change at 222 nm roughly obeyed first-order kinetics, similar to that of ATPase inactivation (data not shown). In addition, binding of S1 to the hydrophobic fluorescent probe, 2-*p*-toluidinylnaphthalene-6-sulfonate, also increased with first-order kinetics (data not shown), suggesting a conformational change which exposes hydrophobic residues.

Time Course of Aggregation of Partially Unfolded S1—Aggregation was monitored at 35°C by measuring turbidity at 350 nm, light scattering at 600 nm and sediment formation under centrifugation at 183,000 × *g* (Fig. 2). Increased light scattering and sedimentation indicates a production of high molecular mass aggregates. However, the turbidity at 350 nm did not increase at all, and sediment appeared transparent (data not shown). The light scattering began to increase after a 5-min lag period, which was followed by a rapid increase for 5–25 min (~12 units/min) and subsequent slowing thereafter (~4 units/min). The time courses were all similar for protein concentrations ranging from 0.06 to 0.48 mg/ml. In this range, the higher concentration made the lag time shorter and the light scattering amplitude larger (data not shown). The S1 concentration in the supernatants from heat-treated samples (Fig. 2, closed circles) decreased slightly for the first 30 min, and more markedly thereafter. On the other hand, when S1 was incubated at 40 or 45°C, where all subdomains of S1 underwent unfolding, the solution became turbid, suggesting formation of an amorphous aggregate. In this case, the time courses of light scattering and turbidity showed a lag time followed by an exponential phase, indicating typical nucleation-dependent polymerization (*32*). Thus, S1 aggregation at 35°C is distinguishable from that occurring at temperatures greater than 40°C.

Dye Binding—The partially unfolded S1 aggregate was characterized by testing its binding to Congo red and Thioflavin T, which are used for amyloid detection (*33–36*). As observed for amyloid, a red shift was observed in the absorbance spectrum of Congo red in the presence of

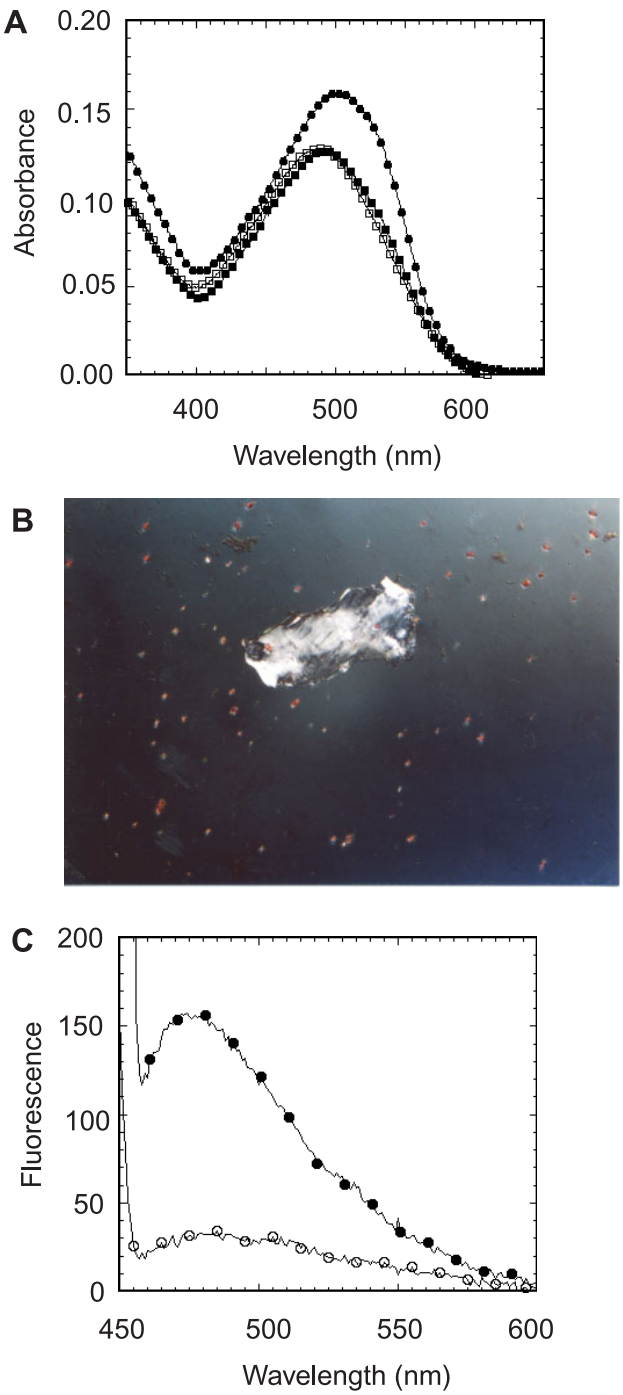

Fig. 3. **Amyloid-like dye-binding properties of the aggregate.** (A) Changes in Congo red absorbance spectrum by the mild heat-treated S1. Congo red alone, open squares; Congo red and native S1, solid squares; Congo red and mild heat–treated S1, solid circles. (B) Polarization micrograph of the aggregate stained with Congo red, ×400. (C) ThioT fluorescence spectra of native (open circles) and mild heat–treated (solid circles) S1s at the excitation wavelength of 440 nm.

heat-treated, but not untreated, S1 (Fig. 3A). Unlike amyloid, the aggregate appeared white and not green-yellow under polarization microscopy (Fig. 3B). The heat-treated S1 also increased fluorescence of ThioT, a fluorescent indicator (Fig. 3C). These interactions of the partially unfolded S1 aggregate with the dyes are similar to those of amyloid.

Size Distribution—The S1 incubated at 35°C for 90 min was observed by electron microscopy using a negative staining method (Fig. 4A). The aggregates were not fibrils but uniformly sized spherical particles with a diameter of ~30 nm. Since no single molecule of native S1 was observed, (native S1 molecule cannot be absorbed onto grids for negative staining), the particles seen on the electron micrographs were oligomers of partially unfolded S1. No fibril-like structure was detected, but the putative fibrils might not be absorbed to grids for the negative staining. However, because the gel filtration analysis indicated that molecular mass of the aggregate was ~600 kDa (see below), suggestive of an oligomer rather than a fibril, the S1 aggregate was likely to comprise spherical particles rather than fibrils. Even after prolonged incubation (7 and 12 h), the spherical particles remained visible but tended to cluster. To examine the effect of long-term incubation on the aggregates, we computationally analyzed the digitized electron micrographs to estimate particle size (Fig. 4B). All samples tested showed a similar distribution of individual particle sizes, especially around the lower area. The results indicate that the size of most particles does not change with the incubation time. It was notable that, despite a long incubation time of 1 week at 4°C, the spherical particles remained the major aggregate component, suggesting that they do not represent an unstable intermediate form (data not shown).

Gel Filtration Analysis of Aggregation—When analyzed by gel filtration, the mild heat-treated samples showed that the major components of the aggregates consisted of three fractions (Fig. 5A): Peak 1 at 6.6 min corresponding to a 580-kDa oligomer; Peak 2 at 7.5 min corresponding to a 310-kDa oligomer; and Peak 3 at 8.9 min corresponding to a 110-kDa protein. Peak 1 and Peak 2 exhibited the 50-kDa subdomain-specific digestion by trypsin and the wavelength shift of the Congo red spectrum (Table 1). In contrast, Peak 3 showed neither trypsin-sensitivity nor any change in the Congo red spectrum (Table 1). These data demonstrate that Peaks 1 and 2 contained oligomers of partially unfolded S1 and that Peak 3 mainly contained monomeric native S1. The fourth, small peak at 11.8 min contained a small amount of myosin light chain dissociated from S1 (data not shown). The yield of the fourth peak did not depend on incubation time. This indicates that the oligomerization is not involved in light chain dissociation.

Figure 5B shows relative peak area as a function of incubation time. The decrease in Peak 3 showed first order kinetics. This is consistent with the kinetics of ATPase inactivation (Fig. 1B). Peak 2 did not increase for the initial 5 min, then increased until ~50 min, and finally reached a steady level. Peak 1 was also at zero for ~5 min, and then continuously increased during incubation. These results suggest that Peak 2 is an intermediate in the process of Peak 1 formation. When the separated Peak 2 was further incubated at 35°C for 2 h without monomeric S1, Peak 1 increased concomitantly as Peak 2 decreased (data not shown), which indicates that the oligomers in Peak 2 may be precursors of those in Peak 1.

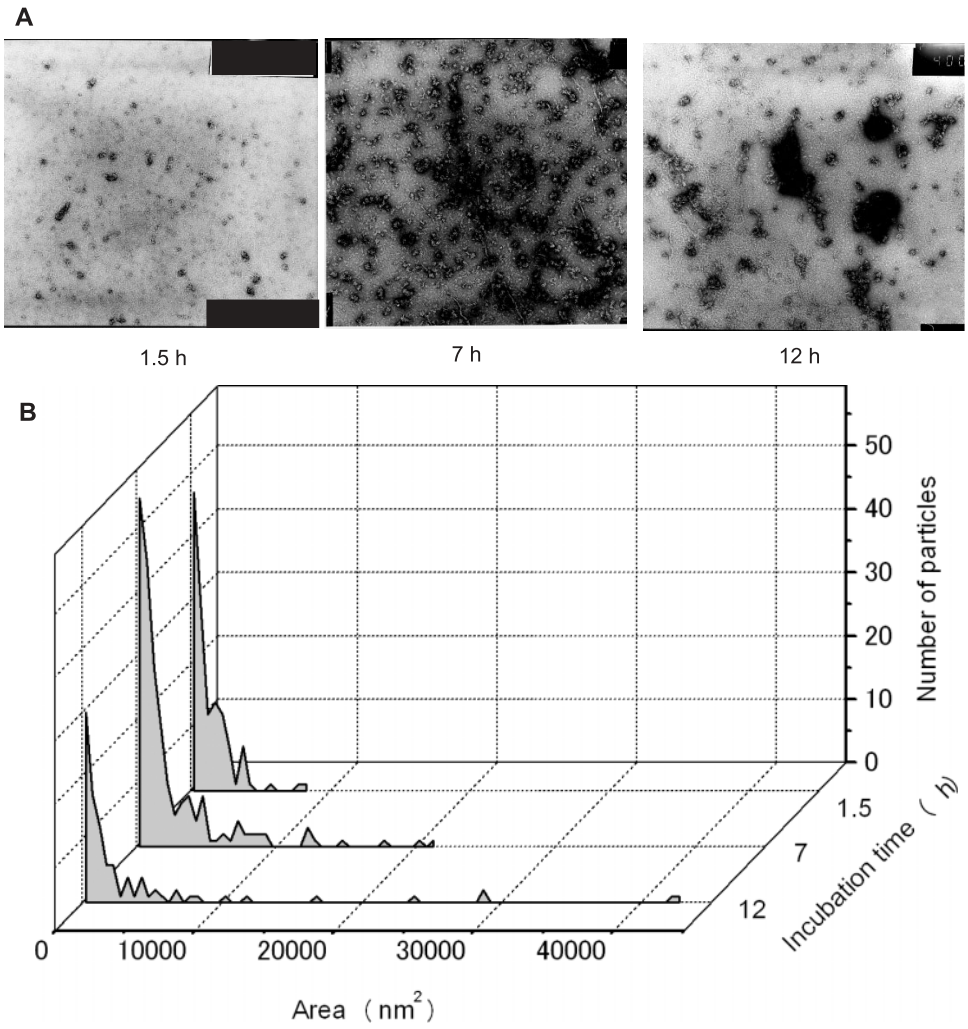

Fig. 4. **Electron micrographs of the aggregate.** (A) S1 incubated at 35°C for 1.5, 7 and 12 h. ×30,000. No molecule of native S1 was seen (see text). (B) Distribution of particle size on the electron micrographs (A). Particle sizes are indicated in terms of the areas measured, as described in "MATERIALS AND METHODS".

Protease Sensitivity—Upon incubation with trypsin, the light scattering of the heat-treated S1 was reduced (data not shown). Molecular mass of the trypsin-treated aggregate analyzed by gel filtration was lower than that of the untreated oligomer (data not shown). These results indicate that the S1 aggregate is protease-sensitive, unlike other typical protease-resistant amyloids.

Aggregation of Isolated 50-kDa Fragment and Its Inhibition by Partially Unfolded S1—To examine the role of the unfolded region in the aggregation of partially unfolded S1, the aggregation of the isolated 50-kDa fragment was examined. When the 50-kDa fragment solution was diluted 60 times in 5 M guanidine-HCl (5 M), it became turbid, suggesting amorphous aggregation. In fact, electron microscopy showed that the aggregated fragments were large and amorphous. The aggregate showed high turbidity at 350 nm with an increase in light scattering at 600 nm. Because the aggregated 50-kDa fragment was highly turbid and thus inappropriate for spectroscopy, the spectrum change of dyes induced by binding of the aggregate could not be examined. The time course of aggregation was S-shaped, with an initial lag-like period of 20 min (Fig. 6, open circles). This lag-like phase partly disappeared upon addition of a small amount of sonicated 50-kDa fragment aggregate as seed (Fig. 6, closed circles), suggesting a nucleation-dependent process. The S1 oligomer did not have a seeding effect, but rather it inhibited the 50-kDa fragment aggregation by decreasing the rate of aggregation, without changing the duration of the lag-like period (Fig. 6, closed squares). Native S1 had little effect on the 50-kDa fragment aggregation (Fig. 6, open squares). Although the aggregation of the 50-kDa fragment may be different from that of partially unfolded S1, these results imply an interaction between the 50-kDa fragment and the partially unfolded S1 oligomer.

DISCUSSION

In this work, we have demonstrated that when unfolded partially, S1 aggregates like other proteins (*2*, *6*, *37–39*). The aggregate has two characteristics. Firstly, the S1 component of the aggregate has a native-like structure as shown by slight changes in CD spectrum. This is consistent with pervious reports that partially unfolded S1

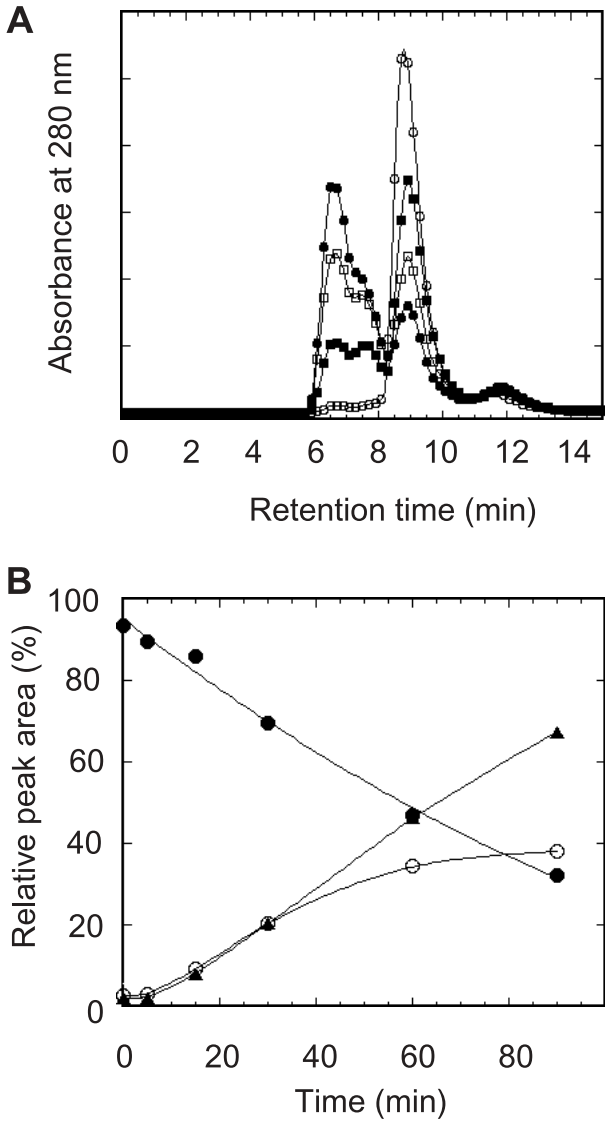

Fig. 5. **Gel filtration analysis of S1 incubated at 35°C.** (A) Incubation periods are 0 (open circles), 30 (solid squares), 60 (open squares) and 90 (solid circles) min, in 0.1 M KCl and 20 mM PIPES (pH 7.0). Samples were filtered through a 0.22-μm pore size membrane, then analyzed by HPLC gel filtration on a TSK G3000SWXL column (TOSOH) with 0.1 M KCl and 20 mM PIPES (pH 7.0) at a flow rate of 1 ml/min. The three major peaks are located at 6.6, 7.5 and 8.9 min, which are named Peaks 1, 2 and 3 respectively. (B) Areas of Peak 1 (closed triangles), Peak 2 (open circles) and Peak 3 (closed circles) obtained from gel filtration, which were calculated by fitting the elution pattern to four normal distributions using ORIGIN software.

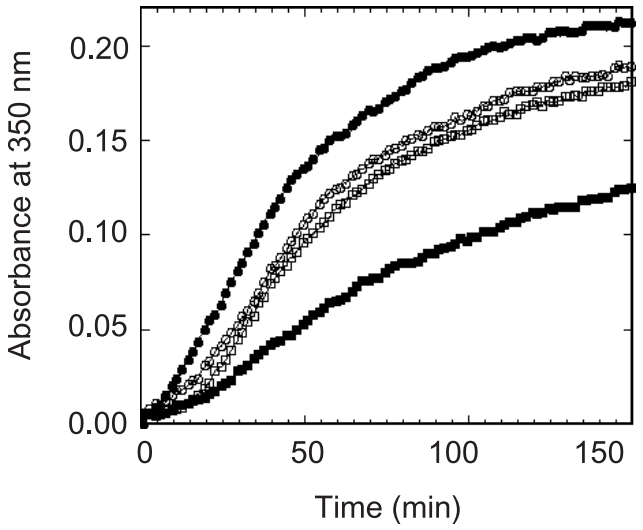

Fig. 6. **Aggregation of the 50-kDa fragment.** The aggregation was monitored by measuring turbidity at 350 nm. To start the aggregation, a solution of 50-kDa fragments (0.044 mg/ml) in 5 M guanidine-HCl containing buffer was diluted with 60 volumes 0.1 M KCl and 20 mM PIPES, pH 7.0 and incubated at 25°C alone (open circles) or in the presence of seed (solid circles), native S1 (open squares) or partially unfolded S1 (solid squares), whose concentrations were 0.0088, 0.02, and 0.02 mg/ml, respectively. These concentrations were 20% of the 50-kDa fragment in molar ratio.

Table 1. **Characterization of the eluted peaks from gel filtration.**

Peak[a]	Molecular mass[b] (kDa)	Sensitivity of 50-kDa subdomain to tryptic digestion[c]	Shift of Congo red spectrum[c]
1	580	+	+
2	310	+	+
3	110	–	–

S1 incubated at 35°C for 60 min was subjected to the gel filtration. The peaks were pooled separately. [a]Peak numbers are indicated as in the legend of Fig. 5. [b]Molecular mass was estimated by reference to elution patterns of molecular weight markers. [c]Each peak was subjected to tryptic digestion followed by SDS-PAGE and spectrum analysis of Congo red.

maintains ATP- and actin-binding functions (*24*, *25*). Like *Saccharomyces cerevisiae* prion Ure2p (*40–42*), the protein aggregation starts from a native-like state with only slight conformational changes. Secondly, the aggregate product is a stable spherical oligomer with amyloid-like, dye-binding properties, and not a conventional fibrillar or an amorphous aggregate. Although some other spherical oligomers has been detected as neurotoxic transient oligomers in amyloid formation (*9–16*), the diameter of S1 oligomer (~30 nm) is larger than those of the transient oligomers (less than 10 nm in many cases) (*10–15*). In addition, the S1 oligomer seems to be more stable than the transient oligomers.

Although the S1 oligomer is not a fibril, it binds to Congo red and Thio T, which are generally used as probes of amyloid fibril formation. As far as Congo red is concerned, the red shift of Congo red spectrum has been ascribed to its intercalation between protein monomers in amyloid fibrils (*43*). A similar spectral shift was observed for the S1 oligomer (Fig. 3A). This suggests that the Congo red is probably bound to the interface between partially unfolded S1 monomers in the aggregate. On the other hand, although the aggregate is birefringent, the Congo red–stained sample appears white under a polarized microscope (Fig. 3B). This is distinct from typical green-yellow birefringence of Congo red bound-amyloid proteins, which is suggestive of the alignment of dyes

along the long axis of fibrils (*44*). Thus, the mode of monomer-monomer contact in S1 oligomer is similar to that in amyloid fibrils, but the arrangement of monomers in S1 oligomer is different from that in amyloid fibrils.

Based on the kinetics and gel filtration analysis, we explain S1 oligomer formation as a sequence of three steps: (1) partial unfolding, (2) formation of an intermediate oligomer, and (3) assembly of intermediates.

$$S1 \xrightarrow{1} S1_{pu} \xrightarrow{2} (S1_{pu})_m \xrightarrow{3} [(S1_{pu})_m]_n$$

where $S1_{pu}$ is the partially unfolded S1, $(S1_{pu})_m$ is an oligomer of m units of the partially unfolded S1, and $[(S1_{pu})_m]_n$ is an oligomer of n units of $(S1_{pu})_m$. Assuming that $(S1_{pu})_m$ and $[(S1_{pu})_m]_n$ correspond to Peaks 2 and 1 in gel filtration, respectively, values of m and n were estimated from the molecular masses in Table 1, 3 for m and 2 for n.

The first order kinetics of partial unfolding (step 1) (Fig. 1B) and the lag time of oligomerization (Figs. 2 and 5B) suggest that the monomeric partially unfolded S1 ($S1_{pu}$) accumulates until its concentration reaches a certain critical level to initiate step 2, which is estimated to be ~0.03 mg/ml: the initial S1 concentration (0.28 mg/ml) multiplied by 10% (inactivation ratio for a lag time of 5 min) (Figs. 1 and 2). This estimate is equal to, or lower than, the critical concentrations of other amyloid aggregations (*45–50*). In step 3, the intermediate of $(S1_{pu})_m$ can assemble into the higher mass oligomer ($[(S1_{pu})_m]_n$).

The final product oligomer ($[(S1_{pu})_m]_n$) cannot assemble any further and remains a spherical particle. This can be attributed to steric hindrance by the bulky native parts (25- and 20-kDa subdomains and light chain) of self-association of the unfolded 50-kDa subdomain. This may also explain how the S1 oligomer inhibits self-aggregation of the isolated 50-kDa fragment without prolonging the nucleating lag-like period (Fig. 6, closed squares). Thus, the S1 oligomer could be incorporated in the nuclei of the 50-kDa fragment aggregates in the lag-like phase, and then native parts of the incorporated S1 could inhibit further association of the 50-kDa fragments.

The explanation of the S1 spheroid formation can be extended to a general mechanism for determining the aggregate morphology of partially unfolded protein. In other words, the bulkiness of native regions and/or steric configuration of native and unfolded regions in partially unfolded proteins may determine whether they associate to form spheroids, fibrils, or something else.

We are grateful to Iwao Ohtsuki and Sachio Morimoto for providing facilities for polarization and electron microscopy, Takuo Yasunaga for comments on image analysis, and Shander Ahmad for reading of the manuscript.

REFERENCES

1. Kelly, J.W. (1998) The alternative conformations of amyloidogenic proteins and their multi-step assembly pathways. *Curr. Opin. Struct. Biol.* **8**, 101–106
2. Guijarro, J.I., Sunde, M., Jones, J.A., Campbell, I.D., and Dobson, C.M. (1998) Amyloid fibril formation by an SH3 domain. *Proc. Natl. Acad. Sci. USA* **95**, 4224–4228
3. Chiti, F., Webster, P., Taddei, N., Clark, A., Stefani, M., Ramponi, G., and Dobson, C.M. (1999) Designing conditions for in vitro formation of amyloid protofilaments and fibrils. *Proc. Natl. Acad. Sci. USA* **96**, 3590–3594
4. Groß, M., Wilkins, D.K., Pitkeathly, M.C., Chung, E.W., Higham, C., Clark, A., and Dobson, C.M. (1999) Formation of amyloid fibrils by peptides derived from the bacterial cold shock protein CspB. *Protein Sci.* **8**, 1350–1357
5. West, M.W., Wang, W., Patterson, J., Mancias, J.D., Beasley, J.R., and Hecht, M.H. (1999) *De novo* amyloid proteins from designed combinatorial libraries. *Proc. Natl. Acad. Sci. USA* **96**, 11211–11216
6. Litvinovich, S.V., Brew, S.A., Aota, S., Akiyama, S.K., Haudenschild, C., and Ingham, K.C. (1998) Formation of amyloid-like fibrils by self-association of a partially unfolded fibronectin type III module. *J. Mol. Biol.* **280**, 245–258
7. Dobson, C.M. (1999) Protein misfolding, evolution and disease. *Trends Biochem. Sci.* **24**, 329–332
8. Horwich, A. (2002) Protein aggregation in disease: a role for folding intermediates forming specific multimeric interactions. *J. Clin. Invest.* **110**, 1221–1232
9. Lansbury, P.T.Jr. (1999) Evolution of amyloid: what normal protein folding may tell us about fibrillogenesis and disease. *Proc. Natl. Acad. Sci. USA* **96**, 3342–3344
10. Volles, M.J., Lee, S.J., Rochet, J.C., Shtilerman, M.D., Ding, T.T., Kessler, J.C., and Lansbury, P.T.Jr. (2001) Vesicle permeabilization by protofibrillar α-synuclein: implications for the pathogenesis and treatment of Parkinson's disease. *Biochemistry* **40**, 7812–7819
11. Lashuel, H.A., Hartley, D., Petre, B.M., Wall, J.S., Simon, M.N., Walz, T., and Lansbury, P.T.Jr. (2003) Mixtures of wild-type and a pathogenic (E22G) form of Aβ40 *in vitro* accumulate protofibrils, including amyloid pores. *J. Mol. Biol.* **332**, 795–808
12. Hoshi, M., Sato, M., Matsumoto, S., Noguchi, A., Yasutake, K., Yoshida, N., and Sato, K. (2003) Spherical aggregates of β-amyloid (amylospheroid) show high neurotoxicity and activate tau protein kinase I/glycogen synthase kinase-3β. *Proc. Natl. Acad. Sci. USA* **100**, 6370–6375
13. Lambert, M.P., Barlow, A.K., Chromy, B.C., Edwards, C., Freed, R., Liosatos, M., Morgan, T.E., Rozovsky, I., Trommer, B., Viola, K.L., Wals, P., Zhang, C., Finch, C.E., Krafft, G.A., and Klein, W.L. (1998) Diffusible, nonfibrillar ligands derived from Aβ1–42 are potent central nervous system neurotoxins. *Proc. Natl. Acad. Sci. USA* **95**, 6448–6453
14. Chromy, B.A., Nowak, R.J., Lambert, M.P., Viola, K.L., Chang, L., Velasco, P.T., Jones, B.W., Fernandez, S.J., Lacor, P.N., Horowitz, P., Finch, C.E., Krafft, G.A., and Klein, W.L. (2003) Self-assembly of Aβ (1–42) into globular neurotoxins. *Biochemistry* **42**, 12749–12760
15. Bucciantini, M., Giannoni, E., Chiti, F., Baroni, F., Formigli, L., Zurdo, J., Taddei, N., Ramponi, G., Dobson, C.M., and Stefani, M. (2002) Inherent toxicity of aggregates implies a common mechanism for protein misfolding diseases. *Nature* **416**, 507–511
16. Walsh, D.M., Klyubin, I., Fadeeva, J.V., Cullen, W.K., Anwyl, R., Wolfe, M.S., Rowan, M.J., and Selkoe, D.J. (2002) Naturally secreted oligomers of amyloid beta protein potently inhibit hippocampal long-term potentiation *in vivo*. *Nature* **416**, 535–539
17. Misawa, S. and Kumagai, I. (1999) Refolding of therapeutic proteins produced in *Escherichia coli* as inclusion bodies. *Biopolymers* **51**, 297–307
18. Clark, E.D. (2001) Protein refolding for industrial processes. *Curr. Opin. Biotechnol.* **12**, 202–207
19. Ajikumar, P.K. and Devaky, K.S. (2001) Solid phase synthesis of hydrophobic difficult sequence peptides on BDDMA-PS support. *J. Pept. Sci.* **7**, 641–649

20. Mihala, N., Bodi, J., Gomory, A., and Suli-Vargha, H. (2001) An alternative solid phase peptide fragment condensation protocol with improved efficiency. *J. Pept. Sci.* **7**, 565–568
21. Speed, M.A., Wang, D.I., and King, J. (1996) Specific aggregation of partially folded polypeptide chains: the molecular basis of inclusion body composition. *Nat. Biotechnol.* **14**, 1283–1287
22. Sellers, J.R. (1999) Myosin, 2nd ed., Oxford University Press, New York
23. Rayment, I., Rypniewski, W.R., Schmidt-Base, K., Smith, R., Tomchick, D.R., Benning, M.M., Winkelmann, D.A., Wesenberg, G., and Holden, H.M. (1993) Three-dimensional structure of myosin subfragment-1: a molecular motor. *Science* **261**, 50–58
24. Setton, A. and Muhlrad, A. (1984) Effect of mild heat treatment on the ATPase activity and proteolytic sensitivity of myosin subfragment-1. *Arch. Biochem. Biophys.* **235**, 411–417
25. Setton, A., Dan-Goor, M., and Muhlrad, A. (1988) Effect of mild heat treatment on actin and nucleotide binding of myosin subfragment 1. *Biochemistry* **27**, 792–796
26. Burke, M., Zaager S., and Bliss, J. (1987) Substructure of skeletal myosin subfragment 1 revealed by thermal denaturation. *Biochemistry* **26**, 1492–1496
27. Perry, S.V. (1955) Myosin adenosinetriphosphatase. *Methods Enzymol.* **2**, 582–588
28. Weeds, A.G. and Taylor, R.S. (1975) Separation of subfragment-1 isoenzymes from rabbit skeletal muscle myosin. *Nature* **257**, 54–56
29. Muhlrad, A. and Morales, M.F. (1984) Isolation and partial renaturation of proteolytic fragments of the myosin head. *Proc. Natl. Acad. Sci. USA* **81**, 1003–1007
30. Bradford, M.M. (1976) A rapid and sensitive method for the quantitation of microgram quantities of protein utilizing the principle of protein-dye binding. *Anal. Biochem.* **72**, 248–254
31. Taussky, H.H. and Shorr, E. (1953) A microcolorimetric method for the determination of inorganic phosphate. *J. Biol. Chem.* **202**, 675–685
32. Harper, J.D. and Lansbury, P.T.Jr. (1997) Models of amyloid seeding in Alzheimer's disease and scrapie: mechanistic truths and physiological consequences of the time-dependent solubility of amyloid proteins. *Annu. Rev. Biochem.* **66**, 385–407
33. Benditt, E.P., Eriksen, N., and Berglund, C. (1970) Congo red dichroism with dispersed amyloid fibrils, an extrinsic cotton effect. *Proc. Natl. Acad. Sci. USA* **66**, 1044–1051
34. Glenner, G.G., Eanes, E.D., and Page, D.L. (1972) The relation of the properties of Congo red-stained amyloid fibrils to the conformation. *J. Histochem. Cytochem.* **20**, 821–826
35. Naiki, H., Higuchi, K., Hosokawa, M., and Takeda, T. (1989) Fluorometric determination of amyloid fibrils in vitro using the fluorescent dye, thioflavin T1. *Anal. Biochem.* **177**, 244–249
36 LeVine, H.III. (1993) Thioflavine T interaction with synthetic Alzheimer's disease β-amyloid peptides: detection of amyloid aggregation in solution. *Protein Sci.* **2**, 404–410
37. Khurana, R., Gillespie, J.R., Talapatra, A., Minert, L.J., Ionescu-Zanetti, C., Millett, I., and Fink, A.L. (2001) Partially folded intermediates as critical precursors of light chain amyloid fibrils and amorphous aggregates. *Biochemistry* **40**, 3525–3535
38. Colon, W. and Kelly, J.W. (1992) Partial denaturation of transthyretin is sufficient for amyloid fibril formation *in vitro*. *Biochemistry* **31**, 8654–8660
39. Lai, Z., Colon, W., and Kelly, J.W. (1996) The acid-mediated denaturation pathway of transthyretin yields a conformational intermediate that can self-assemble into amyloid. *Biochemistry* **35**, 6470–6482
40. Thual, C., Komar, A.A., Bousset, L., Fernandez-Bellot, E., Cullin, C., and Melki, R. (1999) Structural characterization of *Saccharomyces cerevisiae* prion-like protein Ure2. *J. Biol. Chem.* **274**, 13666–13674
41. Bousset, L., Thomson, N.H, Radford, S.E, and Melki, R. (2002) The yeast prion Ure2p retains its native alpha-helical conformation upon assembly into protein fibrils *in vitro*. *EMBO J.* **21**, 2903–2911
42. Bousset, L., Redeker, V., Decottignies, P., Dubois, S., Le Marechal, P., and Melki, R. (2004) Structural characterization of the fibrillar form of the yeast *Saccharomyces cerevisiae* prion Ure2p. *Biochemistry* **43**, 5022–5032
43. Khurana, R., Uversky, V.N, Nielsen, L., and Fink, A.L. (2001) Is Congo red an amyloid-specific dye? *J. Biol. Chem.* **276**, 22715–22721
44. Jin, L.W., Claborn, K.A., Kurimoto, M., Geday, M.A., Maezawa, I., Sohraby, F., Estrada, M., Kaminksy, W., and Kahr, B. (2003) Imaging linear birefringence and dichroism in cerebral amyloid pathologies. *Proc. Natl. Acad. Sci. USA* **100**, 15294–15298
45. Hasegawa, K., Ono, K., Yamada, M., and Naiki, H. (2002) Kinetic modeling and determination of reaction constants of Alzheimer's β-amyloid fibril extension and dissociation using surface plasmon resonance. *Biochemistry* **41**, 13489–13498
46. Lomakin, A., Teplow, D.B., Kirschner, D.A., and Benedek, G.B. (1997) Kinetic theory of fibrillogenesis of amyloid β-protein. *Proc. Natl. Acad. Sci. USA* **94**, 7942–7947
47. Lomakin, A., Chung, D.S., Benedek, G.B., Kirschner, D.A., and Teplow, D.B. (1996) On the nucleation and growth of amyloid β-protein fibrils: detection of nuclei and quantitation of rate constants. *Proc. Natl. Acad. Sci. USA* **93**, 1125–1129
48. Soreghan, B., Kosmoski, J., and Glabe, C. (1994) Surfactant properties of Alzheimer's Aβ peptides and the mechanism of amyloid aggregation. *J. Biol. Chem.* **269**, 28551–28554
49. Wood, S.J., Wypych, J., Steavenson, S., Louis, J.C., Citron, M., and Biere, A.L. (1999) α-Synuclein fibrillogenesis is nucleation-dependent. Implications for the pathogenesis of Parkinson's disease. *J. Biol. Chem.* **274**, 19509–19512
50. Rhoades, E. and Gafni, A. (2003) Micelle formation by a fragment of human islet amyloid polypeptide. *Biophys. J.* **84**, 3480–3487